UNCLASSIFIED
SECURITY CLASSIFICATION OF THIS PAGE

AD-A205019

REPORT DOCUMENTATION PAGE

Form Approved
OMB No. 0704-0188

1a. REPORT SECURITY CLASSIFICATION UNCLASSIFIED	1b. RESTRICTIVE MARKINGS
2a. SECURITY CLASSIFICATION AUTHORITY	3. DISTRIBUTION / AVAILABILITY OF REPORT Approved for public release; distribution unlimited.
2b. DECLASSIFICATION / DOWNGRADING SCHEDULE	
4. PERFORMING ORGANIZATION REPORT NUMBER(S) HDL-TR-2153	5. MONITORING ORGANIZATION REPORT NUMBER(S)
6a. NAME OF PERFORMING ORGANIZATION Harry Diamond Laboratories 6b. OFFICE SYMBOL (If applicable) SLCHD-NW-ES	7a. NAME OF MONITORING ORGANIZATION
6c. ADDRESS (City, State, and ZIP Code) 2800 Powder Mill Road Adelphi, MD 20783-1197	7b. ADDRESS (City, State, and ZIP Code)
8a. NAME OF FUNDING / SPONSORING ORGANIZATION USAF Tactical Shelter System Development Office 8b. OFFICE SYMBOL (If applicable) ESD/AVMS	9. PROCUREMENT INSTRUMENT IDENTIFICATION NUMBER
8c. ADDRESS (City, State, and ZIP Code) Hanscom AFB, MA 01731	10. SOURCE OF FUNDING NUMBERS PROGRAM ELEMENT NO. 64708F; PROJECT NO.; TASK NO.; WORK UNIT ACCESSION NO.

11. TITLE (Include Security Classification)
The Effects of Mounting a Metallic Cylinder Behind a Ground-Plane-Version Electromagnetic Field Sensor

12. PERSONAL AUTHOR(S)
Bruce T. Benwell and Youn M. Lee

13a. TYPE OF REPORT	13b. TIME COVERED	14. DATE OF REPORT (Year, Month, Day)	15. PAGE COUNT
Final	FROM Aug 85 TO Sep 86	January 1989	28

16. SUPPLEMENTARY NOTATION
HDL project: E558E5, AMS code: 6426740000

17. COSATI CODES		
FIELD	GROUP	SUB-GROUP
17	07	

18. SUBJECT TERMS (Continue on reverse if necessary and identify by block number)
See other side.

19. ABSTRACT (Continue on reverse if necessary and identify by block number)

Harry Diamond Laboratories currently uses ground-plane-version electric and magnetic field sensors to measure the electric and magnetic fields produced during a simulated high-altitude electromagnetic pulse (HEMP). The authors have recently fabricated and mounted a hollow metallic cylinder behind the sensor's ground plane to house a fiber-optic transmitter, amplifiers, and other equipment necessary for data collection. The presence of this metallic cylinder increases ("enhances") the amplitude of a signal measured with this new sensor structure geometry ("sensor/cylinder"). The electric and magnetic field enhancements caused by the presence of this metallic cylinder were measured in both the frequency and time domains. The enhancement was also calculated numerically with the use of a three-dimensional finite-difference code.

In the frequency domain, the enhancements for both the electric and magnetic fields were measured with the use of large transverse electromagnetic (TEM) cells. In the time domain, the enhancements were computed by comparing

20. DISTRIBUTION / AVAILABILITY OF ABSTRACT ☒ UNCLASSIFIED/UNLIMITED ☐ SAME AS RPT ☐ DTIC USERS	21. ABSTRACT SECURITY CLASSIFICATION UNCLASSIFIED
22a. NAME OF RESPONSIBLE INDIVIDUAL Bruce T. Benwell	22b. TELEPHONE (Include Area Code) (202) 394-1851
	22c. OFFICE SYMBOL SLCHD-NW-ES

DD Form 1473, JUN 86 Previous editions are obsolete. SECURITY CLASSIFICATION OF THIS PAGE
UNCLASSIFIED

18. SUBJECT TERMS (cont'd)

Field enhancement, electric field sensor, magnetic field sensor, metallic cylinder, shelter, fiber optic system, TEM cell, HEMP sensors, EMP sensors, broad bandwidth EM sensors, electric field enhancement, magnetic field enhancement

19. ABSTRACT (cont'd)

simulated HEMP fields measured with this sensor/cylinder to those measured with miniature electric and magnetic field sensors.

The degree of enhancement of this sensor/cylinder will vary as a function of distance when the sensor/cylinder is placed next to a conducting object, such as a metallic shelter. These enhancements were also investigated with the use of miniature electric and magnetic field sensors.

Contents

Page

1. **Introduction** 5

2. **The Metallic Cylinder** 7

3. **Determining Enhancement Caused by Metallic Cylinder** 9

   3.1 Cylinder Response in Frequency Domain 9
   3.2 Cylinder Response in Time Domain 12
   3.3 Numerical Computation of Cylinder Enhancement 14

4. **Enhancement Caused When Cylinder is Next to Conducting Plane** 16

   4.1 Enhancement Caused When Metallic Cylinder is Placed 0.305 m from an Exterior Shelter Wall 16
   4.2 Enhancement Caused When Metallic Cylinder is Placed 0.305 m from an Interior Shelter Wall 17

5. **Estimation of Field Variation as a Function of Sensor/Cylinder Positioning** 18

6. **Conclusions** 23

References 25

Distribution 27

Figures

1. Fiber-optic cylinder with electric field sensor attached 7
2. End plate of metallic cylinder showing charging port and fiber-optic cable connections 8
3. Metallic cylinder showing transmitter, dc to dc converter, 20-dB Avantec amplifier, bias tee, and electric-field sensor 8
4. Two cylinder orientations for measuring magnetic fields 11
5. Electric-field enhancement [$EF^{E}(f)$] caused by metallic cylinder 12
6. Magnetic-field enhancement [$EF^{H}(f)$] caused by metallic cylinder, with cylinder axis perpendicular to electric field 12

Figures (cont'd)

Page

7. Magnetic-field enhancement [*EFH(f)*] caused by metallic cylinder, with cylinder axis parallel to electric field 12
8. Miniature dipole mounted on a fiber-optic transmitter 13
9. Miniature loop mounted on a fiber-optic transmitter 13
10. Estimation of field variation with sensor/cylinder axis parallel and perpendicular to shelter; tilt angle varied 18
11. Estimation of field variation with sensor/cylinder axis parallel and perpendicular to shelter; distance from shelter varied 20
12. Estimation of field variation with axis of sensor/cylinder parallel to electric field 20
13. Effects of cylinder position on enhancement factors; cylinder is 12 in. from shelter wall, with H_z measured 21
14. Effects of cylinder position on enhancement factors; cylinder is 12 in. from shelter wall, with H_y measured 22

Table 1. Average electric and magnetic field enhancements caused by the metallic cylinder 15

1. Introduction

When measuring the electric and magnetic fields produced by a simulated high-altitude electromagnetic pulse (HEMP), Harry Diamond Laboratories (HDL) currently uses ground-plane-version electric and magnetic field sensors. These sensors are mounted on a 0.218-m circular (8-1/2 in.) aluminum plate that provides both a finite ground plane and a mounting surface for the sensors. Previously, whenever electromagnetic fields were recorded during HEMP simulation, these sensors had been mounted on a 1-m^3 aluminum box ("mapping box"). The 1-m^3 box was needed to shield and contain the recording equipment, such as oscilloscopes and cameras, necessary for data collection.

With the advent of fiber optics, the 1-m^3 box was no longer required and could be replaced by a much smaller and more convenient enclosure. The new enclosure chosen was an aluminum cylinder approximately 0.254 m (10 in.) long, with a diameter of 0.167 m (6-1/2 in.). This size was chosen to allow the electric and magnetic field sensors to be mounted on the metallic cylinder without serious sensor modification and also to shield the transmitter portion of the fiber-optic data link, small signal amplifiers, power supply, and coaxial cables associated with the collection of field data. It will be shown later that the presence of this cylinder increases ("enhances") the amplitude of the signal measured with this new sensor structure geometry (sensor/cylinder). With this metallic cylinder so close to the sensor, it was necessary to examine and characterize the effect of the cylinder on the measurement of electromagnetic fields so that its effect could then be removed.

This report documents the various techniques used to characterize the field perturbation caused by the presence of the metallic cylinder. It will be shown later that the presence of this cylinder increased the amplitude of the measured electromagnetic fields by a constant value for the measured frequency range of 500 kHz to 100 MHz. This perturbation will be referred to as an enhancement. Three different techniques were used to characterize the enhancement. First, the field enhancement caused by the

metallic cylinder as a function of frequency was measured with the use of transverse electromagnetic (TEM) cells with a continuous wave (cw) source. Second, the enhancement was measured in the time domain by comparing electric and magnetic fields measured with a sensor mounted on the metallic cylinder to those measured with miniature sensor mounted directly on a fiber-optic transmitter. Third, the enhancement was calculated numerically with the use of a three-dimensional finite-difference code.

We were also concerned with the effects that a nearby conducting plane (specifically a metallic shelter) would have on the field enhancement of the sensor/cylinder. This effect was investigated along with errors associated with inaccurate positioning of the sensor/cylinder.

2. The Metallic Cylinder

The metallic cylinder was designed specifically to house the transmitter portion of the fiber-optic link, amplifiers, power supply, cables, and other equipment associated with data collection. Additionally, the metallic cylinder's compact size allows greater sensor positional flexibility for measuring electromagnetic fields than did the previously used 1-m^3 box.

Figure 1 shows the metallic cylinder with an electric field sensor attached on one end. The sensor is a top-loaded monopole above an 8-1/2-in. circular aluminum ground plane which is protected with a 1/8-in.-thick fiberglass sheet. The cylinder is constructed from an aluminum tube closed at one end with an aluminum plate. Both the fiber-optic signal and control cables can be attached to the transmitter through this plate. The charging port for the fiber-optic transmitter battery pack can also be accessed through this plate (see fig. 2). The cylinder is exactly 0.263 m (10-1/4 in.) long, with a diameter of 0.163 m (6-3/8 in.). The front end of this cylinder is left open so that an electric or magnetic field sensor can be mounted on it. These sensors can be connected to the fiber-optic transmitter through short coaxial cables. The preamplifiers found in each electric field sensor, along with other small signal amplifiers, if necessary, receive their power directly from the optical transmitter battery pack through a dc to dc converter. Figure 3 shows the metallic cylinder along with equipment that can be placed inside it.

Figure 1. Fiber-optic cylinder with electric-field sensor attached.

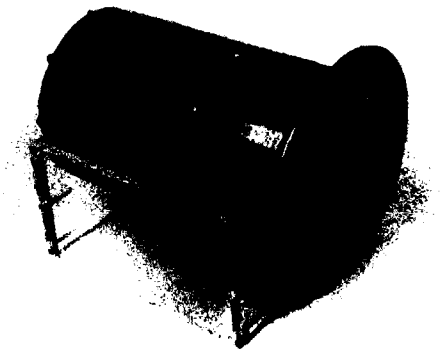

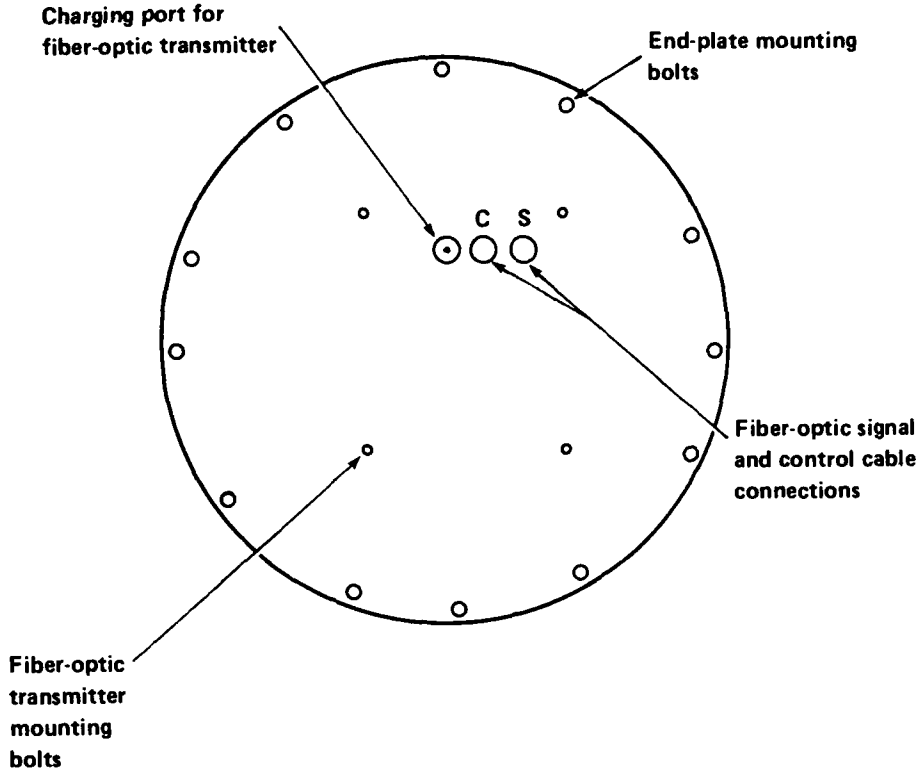

Figure 2. End plate of metallic cylinder showing charging port and fiber-optic cable connections.

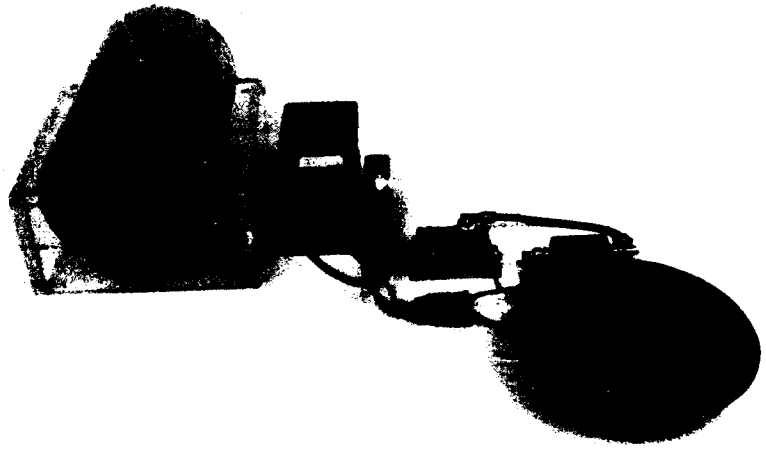

Figure 3. Metallic cylinder showing transmitter, dc to dc converter, 20-dB Avantec amplifier, bias tee, and electric-field sensor.

3. Determining Enhancement Caused by Metallic Cylinder

3.1 Cylinder Response in Frequency Domain

To compute the enhancement caused by the metallic cylinder as a function of frequency, we mounted a field sensor on the cylinder and placed this sensor/cylinder inside large TEM cells. Two separate TEM cells of different sizes were used during this effort. These cells are described in more detail later in this report. The TEM cells provided a uniform TEM field inside each cell. The cells are useful for calibrating low-level sensors and testing equipment emissions and radio-frequency interference (RFI) susceptibility [1].*

The sensor/cylinder was placed midway between the center conductor and the ground plane of the TEM cell by means of a dielectric stand. The TEM cells used for this test are at the National Bureau of Standards in Boulder, CO; these cells provided a constant amplitude field within ±1 dB over the frequencies of interest. The electric and magnetic fields measured by the sensors were transmitted to remotely placed recording equipment through fiber-optic cables. The field enhancements caused by the cylinder were computed by comparing the electric and magnetic fields measured with a sensor mounted on the metallic cylinder to those fields computed at the sensor location without the presence of the sensor/cylinder. The equations used to compute the field enhancement caused by the metallic cylinder are as follows:

$$EF^{E}(f) = \frac{E^{cyl}(f)}{E^{TEM} \times T_1(f)} \quad , \tag{1}$$

$$EF^{H}(f) = \frac{H^{cyl}(f)}{H^{TEM} \times T_2(f)} \quad , \tag{2}$$

*References are listed at the end of the text (see p 25).

$$H^{TEM} = \frac{E^{TEM}}{120\pi} \quad , \tag{3}$$

$$E^{TEM} = \frac{V}{b} \quad , \tag{4}$$

where

$EF^E(f)$, $EF^H(f)$ = the enhancement caused by the cylinder for the electric and magnetic fields, respectively;

$E^{cyl}(f)$, $H^{cyl}(f)$ = the respective electric and magnetic field measured by a sensor mounted on the metallic cylinder;

E^{TEM}, H^{TEM} = the respective electric and magnetic field computed at the center of the TEM cell between the septum and the bottom of the cell without the presence of the cylinder;

$T_1(f)$, $T_2(f)$ = the respective transfer function (ratio of applied field strength to sensor output voltage) of the electric and magnetic field sensors [2];

V = the applied input voltage to the TEM cell for a given frequency; and

b = the separation distance between the center conductor and the bottom of the TEM cell.

The size of one of the TEM cells used was 6 (l) by 3 (w) by 3 (h) m, with the separation between the center conductor and the bottom of the cell being 1.5 m. The cell provides planewave electromagnetic fields inside the cell, and maintains a TEM mode from dc to approximately 40 MHz. A smaller TEM cell was used to cover the frequency range up to 100 MHz. The smaller cell size was 2.4 (l) by 1.2 (w) by 1.2 (h) m, with the distance between the septum and the bottom of the cell being 0.6 m. Because of the size of the cylinder relative to the smaller cell, there was an appreciable interaction between the smaller cell and the metallic cylinder. This interaction was caused by the cylinder's size "impedance loading" the TEM cell, thus changing the characteristic impedance of the cell from 50 ohms [1], and thereby increasing the amplitude of the fields inside the cell. This effect was adjusted by using the enhancement measured in the large cell at the overlapping frequencies between the larger and smaller cell.*

Myron Crawford, National Bureau of Standards, Boulder, Co., recommended this technique on 19 March 1986 during the TEM cell measurements.

For magnetic fields, basically two sensor/cylinder orientations are commonly used for each field component measured. For this reason, the magnetic fields were measured for two angles relative to electric field polarization (Ψ): one with the sensor/cylinder axis parallel to the incident electric field (Ψ = 0 deg), and another with the sensor/cylinder axis normal to the electric field (Ψ = 90 deg). Figure 4 shows two cylinder orientations when the cylinder was used in measuring magnetic fields.

For electric fields, only one sensor/cylinder orientation is possible for each component, that is, with the sensor/cylinder parallel to the electric field.

For electric fields, the average free field enhancement caused by the cylinder was measured to approximately 2.24 with the polarization angle of Ψ = 0 deg. For magnetic fields, the average enhancement was approximately 1.35 for Ψ = 0 deg and 1.26 for Ψ = 90 deg. Figures 5 to 7 show the electric and magnetic field enhancement caused by the metallic cylinder as a function of frequency. As can be seen by these plots, the frequency response of the sensor/cylinder is essentially flat, varying no more than ±1 dB from the selected average value. The standard deviation for the electric field enhancement was 0.5 dB, and for the magnetic field enhancement, was 0.3 dB for Ψ = 0 deg and 0.6 dB with Ψ = 90 deg.

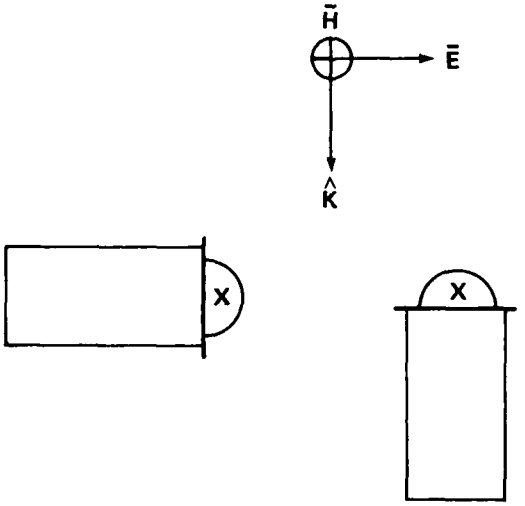

Figure 4. Two cylinder orientations for measuring magnetic fields (cylinder parallel and perpendicular to E-field polarization). (Both orientations are measuring H-field component into page.)

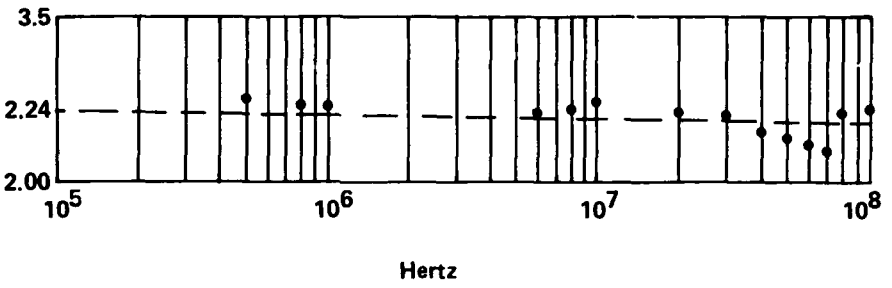

Figure 5. Electric-field enhancement [$EF^E(f)$] caused by metallic cylinder. Dashed line represents average value of enhancement.

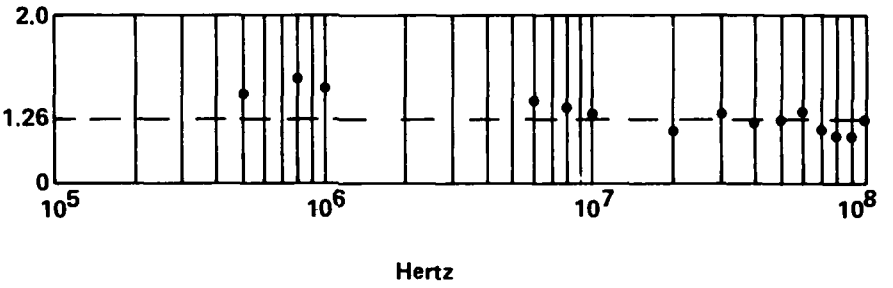

Figure 6. Magnetic-field enhancement [$EF^H(f)$] caused by metallic cylinder, with cylinder axis perpendicular to electric field. Dashed line represents average value of enhancement.

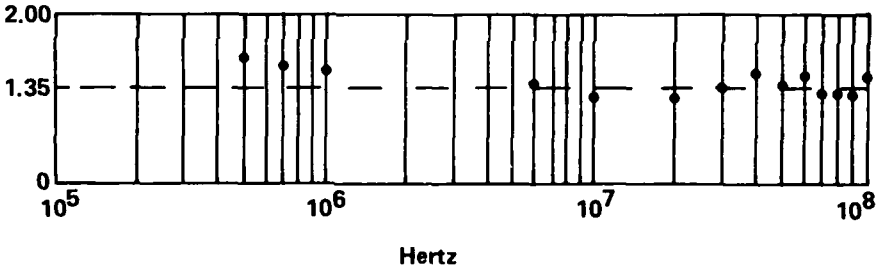

Figure 7. Magnetic-field enhancement [$EF^H(f)$] caused by metallic cylinder, with cylinder axis parallel to electric field. Dashed line represents average value of enhancement.

3.2 Cylinder Response in Time Domain

To compute the enhancement caused by the metallic cylinder in the time domain, a series of tests were performed with the Army Electromagnetic Pulse Simulator Operations (AESOP) in Woodbridge, VA. AESOP is a full-threat-level fixed-site HEMP simulator. Using basically a 7-MV pulse generator and 300-m horizontal biconic radiating antenna, AESOP can produce a radiated free field from 20 to 50 kV/m at 50 m from the pulser. The pulse output from AESOP is a double-exponential with a frequency content up to approximately 125 MHz.

To measure the electric and magnetic field enhancement caused by the metallic cylinder in the time domain, we first had to design and construct miniature electric and magnetic field sensors that would attach directly to

the front end of the fiber-optic transmitter (0.083 (w) by 0.103 (h) by 0.147 (l) m). This design allowed the transfer function (ratio of applied field strength to sensor output voltage) of the sensor mounted on the transmitter to be measured as a whole by placing this entire package in a TEM cell (2 (l) by 0.67 (h) by 1 (w) m). The TEM cell used to measure the transfer function of the sensor mounted to the transmitter was located at HDL. These sensors can be seen figures 8 and 9.

We have already determined through frequency domain analysis that the enhancement caused by the metallic cylinder is reasonably flat over the measured frequency range (with a standard deviation of 0.5 dB for electric fields and 0.3 dB for magnetic fields); also, as expected, there was no appreciable visible change in waveshape between AESOP fields measured with the miniature sensor mounted on a fiber-optic transmitter and those

Figure 8. Miniature dipole mounted on a fiber-optic transmitter.

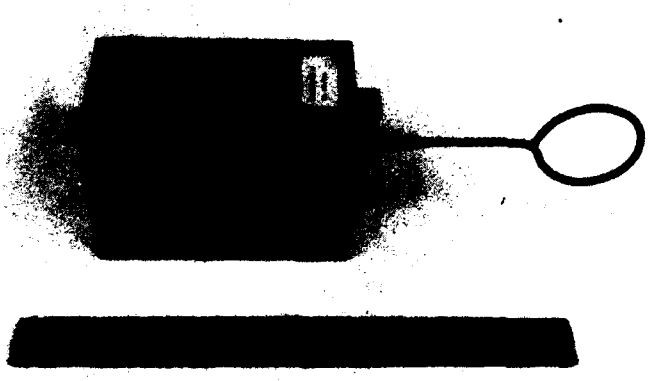

Figure 9. Miniature loop mounted on a fiber-optic transmitter.

measured with the sensor/cylinder. It was therefore concluded that any lengthy data processing could be eliminated and that simply comparing the peak amplitudes of the fields measured with the miniature sensor mounted on the transmitter to those measured with the sensor/cylinder was sufficient to characterize the enhancement caused by the cylinder in the time domain.

To compute the magnetic field enhancement caused by the metallic cylinder, the radial component of the magnetic field from the AESOP radiator was measured with the small magnetic field sensor mounted on a fiber-optic transmitter. The miniature sensor mounted on the transmitter was then replaced with the sensor/cylinder to measure the same field component. The ratio of the peak amplitude measured by the sensor/cylinder to that measured by the miniature sensor mounted on the transmitter represents the magnetic field enhancement caused by the metallic cylinder. This value was 1.25 with the metallic cylinder both normal and parallel to the electric field.

To compute the electric field enhancement caused by the metallic cylinder, the horizontal electric field from the AESOP radiator was measured with a miniature electric field sensor mounted on a fiber-optic transmitter. The miniature sensor mounted on the transmitter was then replaced with the sensor/cylinder to measure the same horizontal electric field component. The ratio of the peak amplitude of these two waveforms represents the electric field enhancement caused by the cylinder; this value was 2.00. The major axis of the sensor/cylinder was parallel to the electric field.

All time-domain enhancement measurements were made at a height of 6 m above earth ground. This provided at least 20 ns of "clear time" in the incident pulse before the ground reflection occurred, and thus allowed the peak of the incident electric and magnetic fields to be measured, better simulating free-field conditions.

3.3 Numerical Computation of Cylinder Enhancement

The enhancement caused by the metallic cylinder was numerically computed using a three-dimensional (3-D) finite-difference, static time domain solution to Maxwell's equations [3]. A spatial grid interval of 1 in. was

used to model the cylinder and its boundary. The enhancement factor was determined by first generating a static field in the absence of the cylinder, next introducing the cylinder into the static field, and then taking the ratio of the computed static field level changes (present at one end of the cylinder) with and without the cylinder present.

As mentioned earlier, each sensor is mounted on an 8-1/2-in. circular aluminum plate to provide a finite ground plane and a mounting surface for the sensor. Because of this plate, the sensor had to be modeled in two ways. In the first model, the sensor plate was omitted. For this case, the electric-field enhancement factor was 2.27. For the magnetic field, the enhancement factor was 1.28 for both $\Psi = 0$ deg and $\Psi = 90$ deg. In the second model, the flange was 1 in. thick. The model did not allow for a more accurate representation of the plate thickness. In this case the electric-field enhancement was 1.9. For magnetic fields the enhancement factor was 1.16 for both $\Psi = 0$ deg and $\Psi = 90$ deg [3].

In reality, the flange thickness is only 0.125 in. One would conclude that the actual enhancement would be bounded by the values obtained from modeling the sensor/cylinder with and without the mounting flange. Table 1 summarizes the derived free-field enhancement factors for the fiber-optic cylinder.

Table 1. Average electric and magnetic field enhancements caused by the metallic cylinder

Field	cw	Numerical[a]	Pulse
Electric	2.24	2.27[b]	2.00
		1.90[c]	
Magnetic	1.26	1.28[b]	1.25
		1.16[c]	

[a] *Computer modeled using 3-D finite-difference code [3].*

[b] *Modeled without flange.*

[c] *Modeled with 1-in. flange.*

4. Enhancement Caused When Cylinder is Next to Conducting Plane

When the metallic cylinder is placed next to a conducting plane, such as a large metallic enclosure, the enhancement of the electric and magnetic fields will change. This change is dependent on both distance from the conducting surface and orientation of the sensor/cylinder. At the time of this investigation, we were concerned with the cylinder enhancement when the sensor/cylinder was placed 0.305 m (12 in.) from an Army S280C shelter. The sensor/cylinder was used to measure the HEMP shielding effectiveness (insertion loss) of an S280C shelter [4]. An S280C shelter is a double-skinned aluminum enclosure approximately 2.3 by 2.3 by 3.7 m.

4.1 Enhancement Caused When Metallic Cylinder is Placed 0.305 m (12 in.) from an Exterior Shelter Wall

To measure the electric and magnetic field enhancements caused when the cylinder is placed 0.305 m from the shelter, we again used the miniature electric and magnetic field sensors, as mentioned earlier, that would attach directly to the front end of the fiber-optic transmitter. The miniature sensor mounted on the transmitter was placed 0.305 m from the rear of the shelter, and electric and magnetic fields were recorded. The miniature sensor mounted on the fiber-optic transmitter was then replaced by the sensor/cylinder, and the electric and magnetic fields were again recorded. The ratio of the peak amplitudes of the fields measured with the sensor mounted on the transmitter to those measured with the sensor/cylinder was 1.86 for electric fields and 1.17 for magnetic fields. These values represent the electric and magnetic field enhancements caused by the cylinder at this location.

When the miniature sensor was mounted on the transmitter it was basically assumed that the interactions between the miniature sensor and the shelter could be neglected. This assumption is justified since the longest dimension of the miniature sensor mounted on the transmitter is approximately 0.05 λ at 100 MHz, the highest frequency of interest, where λ

is the wavelength. Also, the volume of the miniature sensor mounted on a transmitter is only 5.2×10^{-5} times that of the shelter. Again, peak amplitudes were used to determine the enhancement caused by the cylinder in the time domain since there was no appreciable change in waveshape between the fields measured with the miniature sensor mounted on the transmitter and those measured with the sensor/cylinder.

4.2 Enhancement Caused When Metallic Cylinder is Placed 0.305 m (12 in.) from an Interior Shelter Wall

The electric and magnetic field enhancements when the sensor/cylinder was placed inside the shelter were derived with the same procedures used for the external enhancements. When the responses of the miniature electric and magnetic field sensors mounted on a transmitter were compared to those of the sensor/cylinder, the electric and magnetic field enhancements caused by the metallic cylinder placed 0.305 m from the internal shelter wall were 1.89 and 1.4, respectively.

5. Estimation of Field Variation as a Function of Sensor/Cylinder Positioning

To determine if a measured signal is sensitive to sensor/cylinder positioning next to a conducting plane, electric and magnetic fields were measured as a function of sensor/cylinder distance from an S280C shelter. The effects of misaligning the sensor/cylinder were also studied.

Peak amplitude variation caused by sensor/cylinder positioning error was first examined by measuring magnetic fields while the angle of the sensor/cylinder axis was varied with respect to the shelter wall. The plane containing the magnetic field sensor was held fixed so that the sensor was still measuring the same magnetic field component. With the sensor/cylinder angle varied up to 30 deg from a vertical position (sensor/cylinder parallel to the shelter wall and perpendicular to the electric field polarization — see fig. 10a), the peak amplitude varied less than 0.6 percent. The peak amplitude variation was 1.6 percent when the sensor/cylinder angle was varied up to 30 deg from a horizontal position (sensor/cylinder perpendicular to the shelter wall and parallel to the electric field polarization — see fig. 10b). During these measurements, there were no appreciable changes in pulse waveshape.

Figure 10. Estimation of field variation with sensor/cylinder axis (a) parallel and (b) perpendicular to shelter; tilt angle varied.

(a)

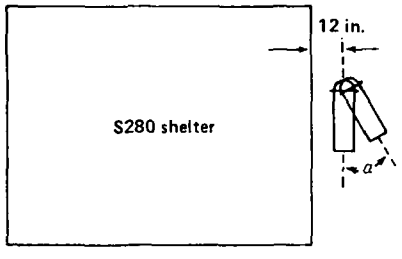

α (deg)	Peak amplitude (A/m)
0	105.6
20	105.1
30	105.7

(b)

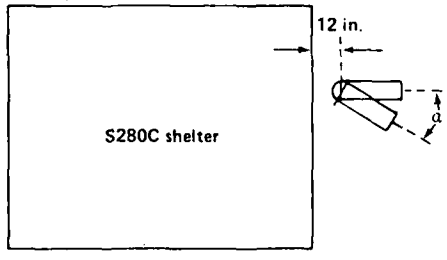

α (deg)	Peak amplitude (A/m)
0	112.1
20	110.3
30	111.8

Variations of the peak magnetic field were also measured as a function of distance between the shelter wall and the sensor/cylinder. With the axis of the sensor/cylinder parallel to the shelter, peak amplitudes varied approximately 7 percent when the sensor/cylinder distance was varied from 0.127 to 0.305 m (5 to 12 in., see fig. 11a). With the sensor/cylinder axis perpendicular to the shelter wall, and the distance varied from 0.064 to 0.305 m (2.5 to 12 in.), peak amplitudes varied approximately 8 percent (fig. 11b). There was no appreciable change in waveshape during these measurements.

When a desired magnetic field component is measured, the sensor/cylinder axis can be either perpendicular or parallel to the shelter. However, electric field sensors do not have these two degrees of freedom. The axis of the sensor/cylinder must always be parallel with the desired field component. The amplitude of the electric field varied approximately 61 percent (without appreciable change in waveshape) when the sensor/cylinder distance was varied from 0.019 to 0.254 m (3/4 to 10 in., see fig. 12). Note that a small positioning error leads to a large variation in peak amplitude of the electric field when the sensor/cylinder is placed very close (less than 0.152 m (6 in.)) to the shelter. The peak amplitude of the electric field varied less than 10 percent when the sensor/cylinder was varied from 0.152 to 0.254 m (6 to 10 in.).

Some significant results have been determined through these tests. As shown by measurements taken with the sensor/cylinder 0.305 m from the shelter, there is at least a 6.2 percent increase in the measured peak magnetic field with the sensor/cylinder parallel to the electric field, as compared to the measured field with the sensor/cylinder perpendicular to the electric field. A major contribution to this measured field increase is due to a portion of the currents induced on the surface of the cylinder by the electric field coupling to the magnetic field sensor. Figures 13 and 14 show the results of this effect.

To summarize, when the sensor/cylinder axis is normal to a shelter wall and the electric field polarization is parallel to the sensor/cylinder axis, appreciable field enhancements will occur for magnetic fields. When the axis of the sensor/cylinder is oriented parallel to the shelter wall and the electric field is polarized perpendicular to the sensor/cylinder, enhancement caused by the electric field is minimized. These results were also confirmed numerically [5].

(a)

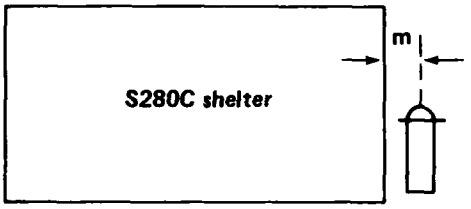

m (in.)	Peak amplitude (A/m)
5	113.2
6	109
8	105.3
10	106.3
12	105.6

(b)

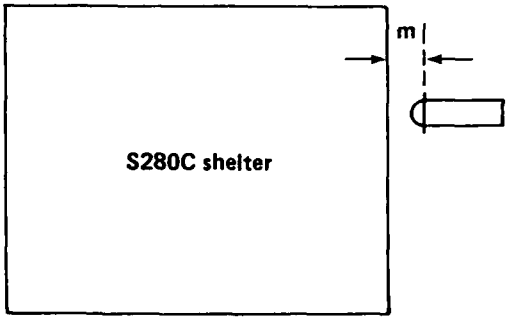

m (in.)	Peak amplitude (A/m)
2.5	122.0
3	115.7
4	114.1
12	112.1

Figure 11. Estimation of field variation with sensor/cylinder axis (a) parallel and (b) perpendicular to shelter; distance from shelter varied.

Figure 12. Estimation of field variation with axis of sensor/cylinder parallel to electric field; distance from shelter varied.

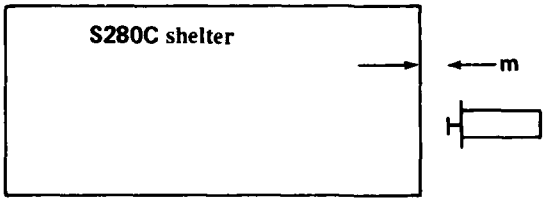

m (in.)	Peak amplitude (kV/m)
0.75	210
2.5	112.8
4	92.5
6	91.4
8	82.8
10	82.4

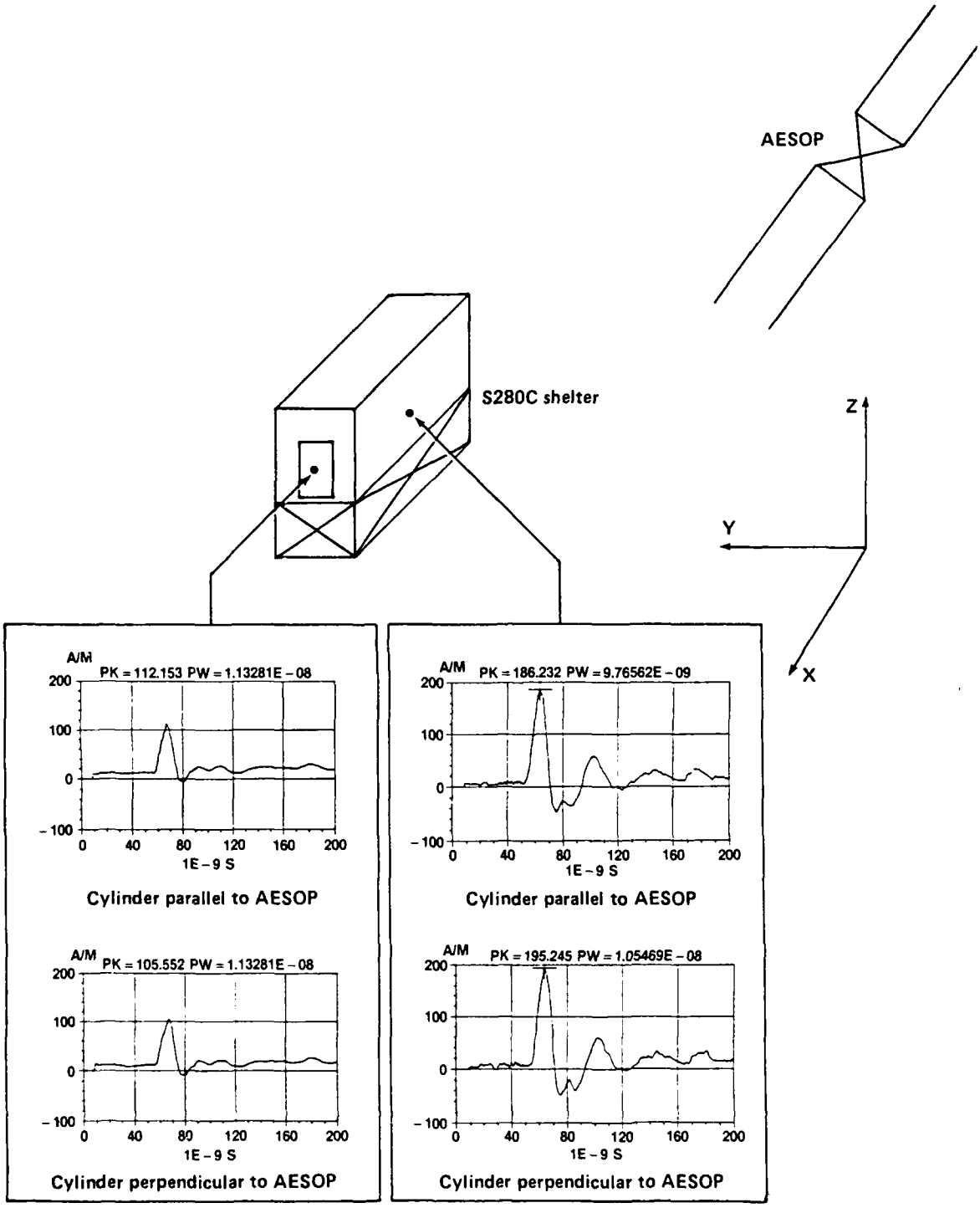

Figure 13. Effects of cylinder position on enhancement factors. Cylinder is 12 in. from shelter wall, with H_z (horizontal component of surface current) measured. Cylinder is either parallel to AESOP antenna (x-axis) or perpendicular to AESOP antenna (y-axis).

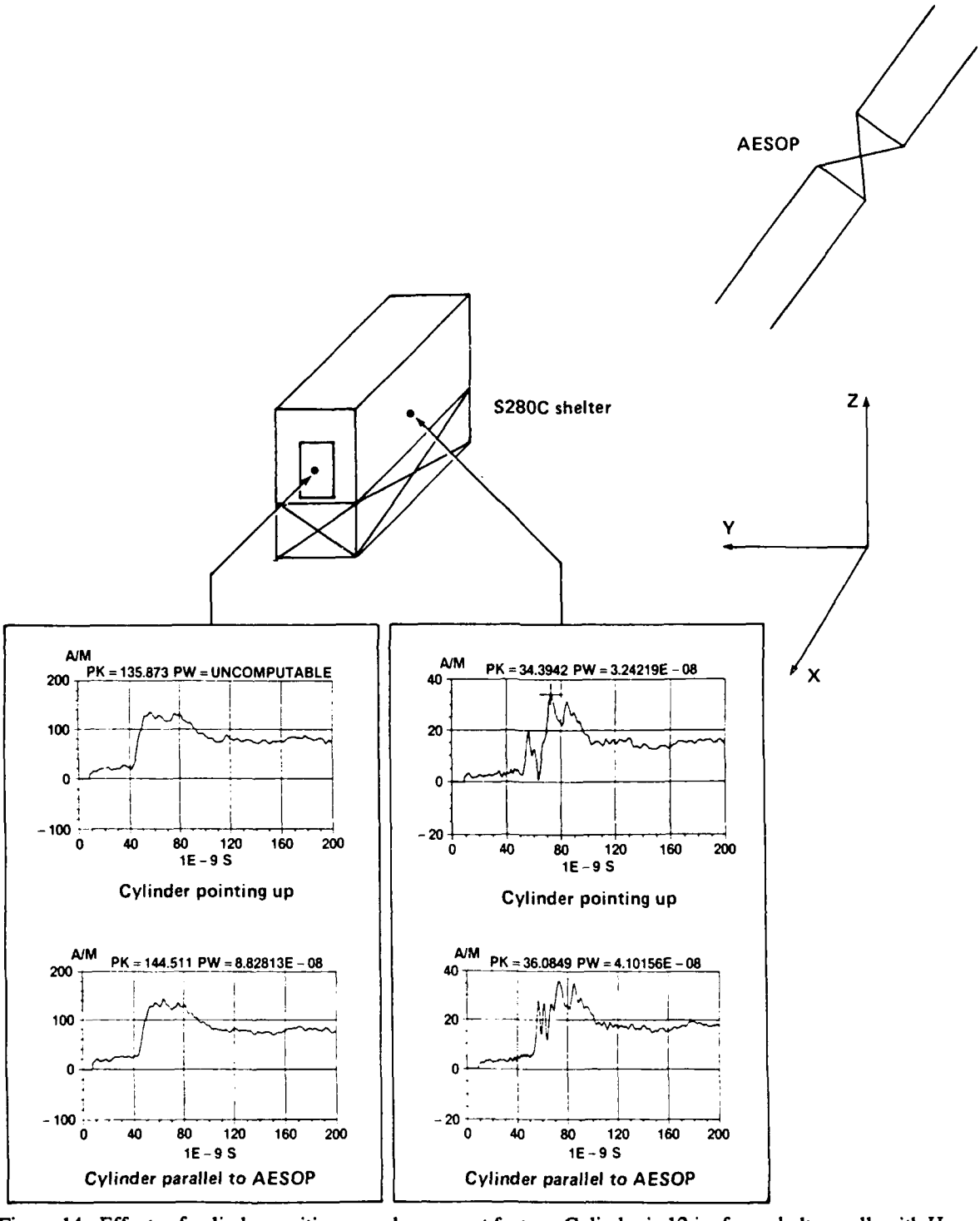

Figure 14. Effects of cylinder position on enhancement factors. Cylinder is 12 in. from shelter wall, with H_y (vertical component of surface current) measured. Cylinder is either pointing up (z-axis) or parallel to AESOP antenna (x-axis).

6. Conclusions

Mounting a field sensor to the metallic cylinder, as described in this report is a very convenient technique for recording electromagnetic fields. It has been shown that the presence of this metallic cylinder causes a field enhancement which is linear over the frequency range measured. This enhancement varies by no more than ±1 dB from the average value, with a standard deviation of 0.5 dB for electric fields and 0.3 dB for magnetic fields.

The field enhancement caused by the presence of the metallic cylinder has been investigated through three independent methods. The enhancements caused by the metallic cylinder were determined to be 2.24 for electric fields and 1.26 for magnetic fields in free field (i.e., without the presence of a conducting plane) based on the cw/frequency-domain measurements. Of the three methods discussed, the frequency domain method was chosen to best estimate the enhancement caused by the cylinder because of the controlled environment and accuracy to which fields were recorded during testing. Table 1 shows the enhancements derived for the three methods.

Testing has shown that improperly aligning the sensor/cylinder during the measurement of a magnetic field has a minimal effect on the measured signal. A sensor/cylinder misalignment of 30 deg will introduce perturbations of only less than 2 percent. On the other hand, the sensor/cylinder is sensitive to position as a function of distance from the shelter wall, because the enhancement caused by the cylinder changes as a function of distance. This effect can be minimized by defining sensor location to be at least 0.152 m (6 in.) from the shelter.

When the sensor/cylinder is used to measure surface current or to infer shielding effectiveness (SE), interactions occurring between the sensor/cylinder and conducting plane (i.e., a metallic shelter) can be minimized by the following procedures.

(1) Place the sensor/cylinder at least 6 in. from the shelter wall (12 in. has shown to be a convenient distance, one consistent with other practiced shielding methods).

(2) Avoid placing the sensor/cylinder perpendicular to the shelter wall for magnetic field measurements.

(3) Avoid placing the sensor/cylinder parallel to the electric field polarization for magnetic field measurements. Disregard this rule for measurements for which the only remaining cylinder position is perpendicular to the shelter wall.

References

(1) Myron L. Crawford, *Generation of Standard EM Fields Using TEM Transmission Cells,* IEEE Trans. Electromag. Compat., Vol. EMC-16, No. 4 (November 1974).

(2) Youn M. Lee and Bruce T. Benwell, *Calibration Techniques and Procedures for SRI's Electric and Magnetic Field Sensors,* Harry Diamond Laboratories report, to be published.

(3) Terry H. Rudolph and R. A. Perala, *Numerical Analysis of the Response of an S280C Shelter to a Nuclear Electromagnetic Pulse Environment,* EMA, Inc., HDL-CR-83-023-1, under contract to Harry Diamond Laboratories (December 1983).

(4) Youn M. Lee and Bruce T. Benwell, *Simulated High Altitude Electromagnetic Pulse Test on DoD Standard Family of Tactical Shelters — Part 1: Analysis,* Harry Diamond Laboratories, HDL-TR-2104 (July 1988).

(5) Paul A. McKenna and R. A. Perala, *Numerical Analysis of the Response of an S280C Shelter to a Simulated NEMP Environment and the Effects of Nearby Groundplane on Electromagnetic Sensor Enhancement Factors,* EMA, Inc., EMA-85-R-17 (December 1984).

DISTRIBUTION

ADMINISTRATOR
DEFENSE TECHNICAL INFORMATION CENTER
ATTN DTIC-DDA (12 COPIES)
CAMERON STATION, BLDG 5
ALEXANDRIA, VA 22304-6145

AFTSSDO
ESD/AVMS (5 COPIES)
HANSCOM AFB, MA 01731

HQ CECOM (DRSEL-ED-SS) (5 COPIES)
FT MONMOUTH, NJ 07703

HQ USMC
CMC (LME-1) (5 COPIES)
WASHINGTON, DC 20380

USA NATICK RESEARCH &
DEVELOPMENT CENTER
ATTN (STRNC-UST) (5 COPIES)
NATICK, MA 01760

NAVAL AIR SYSTEMS COMMAND
NAVAIR 41712A (5 COPIES)
WASHINGTON, DC 20361

HQ ESC/LGMG (3 COPIES)
KELLY AFB, TX 78241

HQ AFCC/LGMB (3 COPIES)
SCOTT AFB, IL 62225

HQ TAC/LGKS (3 COPIES)
LANGLEY AFB, VA 23665

AFMMFO/FOL (3 COPIES)
FT DETRICK, MD 21701

HQ USAFE/LGME (3 COPIES)
APO NY 09012

AAC/OLAA (3 COPIES)
HANSCOM AFB, MA 01731

TAFIG/IIAC (3 COPIES)
LANGLEY AFB, VA 23665

HQ 9 AF/LGMA (3 COPIES)
SHAW AFB, SC 29152

HQ USAF/SGHR (3 COPIES)
BOLLING AFB
WASHINGTON, DC 20332

HQ SAC/DEP (3 COPIES)
OFFUTT AFB, NE 68113

AD/YIL (3 COPIES)
EGLIN AFB, FL 32542

AFESC/RDCS (3 COPIES)
TYNDALL AFB, FL 32403

HQ AFLC/LOC/CFSW (2 COPIES)
WRIGHT-PATTERSON AFB, OH 45433

RADC/RBES (2 COPIES)
GRIFFISS AFB, NY 12241

NCEL (CODE L55) (2 COPIES)
PORT HUENEME, CA 93043

HQ DEPT OF ARMY
SARD-TN (2 COPIES)
SARD-ZCA
WASHINGTON, DC 20310

US ARMY (CERL) (2 COPIES)
PO BOX 4005
CHAMPAIGN, IL 61820

BRDC/DRDME-EME (2 COPIES)
FT BELVOIR, VA 22060

US ARMY
TACOM/DRSTA-RSR (2 COPIES)
WARREN, MI 48090

HQ USAF/RDPT (2 COPIES)
BOLLING AFB
WASHINGTON, DC 20330

HQ DCA
J300 (2 COPIES)
WASHINGTON, DC 20305

DCA
CODE 900 (2 COPIES)
WASHINGTON, DC 20305

EMA
ATTN R. PERALA, J. ELLIOTT (2 COPIES)
PO BOX 26
DENVER, CO 80226-0263

MRC
ATTN W. STARK (2 COPIES)
4935 N. 30TH STREET
COLORADO SPRINGS, CO 80919-3156

SOL TELECOMMUNICATIONS
ATTN S. CLARK
PO BOX 4070
WOODBRIDGE, VA 22194

US ARMY LABORATORY COMMAND
ATTN TECHNICAL DIRECTOR, AMSLC-CT

DISTRIBUTION (cont'd)

INSTALLATION SUPPORT ACTIVITY
ATTN LEGAL OFFICE SLCIS-CC
ATTN S. ELBAUM, SLCIS-CC-IP

USAISC
ATTN RECORD COPY, ASNC-ADL-TS
ATTN TECHNICAL REPORTS BRANCH,
ASNC-ADL-TR (2 COPIES)

HARRY DIAMOND LABORATORIES
ATTN DIRECTOR, SLCHD-D
ATTN D/DIVISION DIRECTORS
ATTN ASSOC DIRECTOR, SLCHD-PO
ATTN DIRECTOR, SLCHD-ST
ATTN DIRECTOR, SLCHD-TA
ATTN DIRECTOR, SLCHD-TS
ATTN DIRECTOR, SLCHD-NW
ATTN DEPUTY DIRECTOR, SLCHD-NW-E
ATTN LIBRARY, SLCHD-TL (3 COPIES)
ATTN LIBRARY, SLCHD-TL (WOODBRIDGE)
ATTN CHIEF, SLCHD-NW-EP
ATTN CHIEF, SLCHD-NW-EH
ATTN CHIEF, SLCHD-NW-ES
ATTN CHIEF, SLCHD-NW-TN
ATTN CHIEF, SLCHD-NW-RP

HARRY DIAMOND LABORATORIES (cont'd)
ATTN CHIEF, SLCHD-NW-CS
ATTN CHIEF, SLCHD-NW-TS
ATTN CHIEF, SLCHD-NW-RS
ATTN CHIEF, SLCHD-NW-P
ATTN H. LESSER, SLCHD-IT-ED
ATTN W. L. VAULT, SLCHD-NW
ATTN R. J. CHASE, SLCHD-NW-EP (2 COPIES)
ATTN W. O. COBURN, SLCHD-NW-EP
ATTN A. HERMANN, SLCHD-NW-EP
ATTN C. KENYON, SLCHD-NW-EP
ATTN C. LE, SLCHD-NW-EP
ATTN B. LUU, SLCHD-NW-EP
ATTN C. REIFF, SLCHD-NW-EP
ATTN D. TROXEL, SLCHD-NW-EP
ATTN J. BRACKETT, SLCHD-NW-ES
ATTN J. LATESS, SLCHD-NW-ES
ATTN W. J. SCOTT, SLCHD-NW-ES (5 COPIES)
ATTN T. R. FLORY, SLCHD-NW-P
ATTN K. WARNER, SLCHD-NW-P
ATTN R. POLIMADEI, SLCHD-NW-P
ATTN J. W. MILLER, JR., SLCHD-TA-SS
ATTN B. T. BENWELL, SLCHD-NW-ES
(10 COPIES)
ATTN Y. M. LEE, SLCHD-NW-ES (2 COPIES)